Available online at www.sciencedirect.com

ScienceDirect

Mendeleev Commun., 2022, **32**, 504–506

Mendeleev Communications

Hemoglobin conformation detection by Raman spectroscopy on single human red blood cells captured in a microfluidic chip

Georgii V. Grigorev,*[a,b] Alexander V. Lebedev,[c] Xiaohao Wang,[d] Xiang Qian,*[d] Georgii V. Maksimov,[e,f] Evgenia U. Parshina[e] and Liwei Lin[b]

[a] *Tsinghua Berkeley Shenzhen Institute, Tsinghua University, 518055 Shenzhen, China. E-mail: georgii@berkeley.edu*
[b] *Mechanical Department, University of California in Berkeley, Berkeley, CA 94703, USA*
[c] *Machine Building Department, N. E. Bauman Moscow State Technical University, 105005 Moscow, Russian Federation*
[d] *Shenzhen International Graduate School, Tsinghua University, 518055 Shenzhen, China. E-mail: qian.xiang@sz.tsinghua.edu.cn*
[e] *Department of Biology, M. V. Lomonosov Moscow State University, 119991 Moscow, Russian Federation*
[f] *National University of Science and Technology 'MISIS', 119049 Moscow, Russian Federation*

DOI: 10.1016/j.mencom.2022.07.024

The Raman spectrum of a single erythrocyte captured by a microfluidic chip was recorded to determine the conformation of hemoglobin under conditions similar to the hemodynamics of a blood vessel. Amplitude changes in the Raman spectrum at 1355, 1375, 1552, 1620, 1585 and 1637 cm^{-1} reflect changes in pO_2 due to O_2 binding to hemoglobin heme.

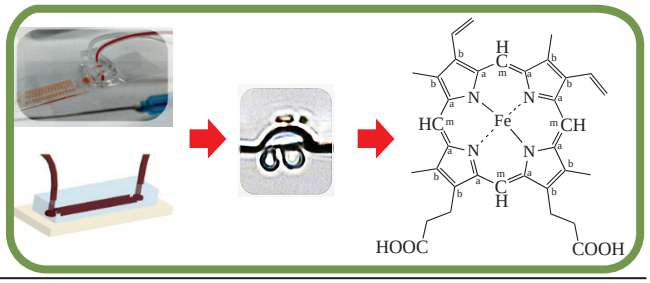

Keywords: microfluidics, Raman spectroscopy, RBC, erythrocyte, hemoglobin, conformation.

For the analysis of cells and tissues *in situ*, microfluidic devices have been developed over the past decades.[1] Recently, optical and physical research methods have been integrated with microfluidics platforms, enabling innovative research. For example, the rheological properties of single-cell membranes have been used to analyze fertility[2] by evaluating the adhesion and deformability of red blood cells (RBCs) in physiological flows.[3] These microfluidic platforms are usually made of polydimethylsiloxane (PDMS) as a construction material because it is inexpensive and easy to attach to another PDMS part or glass material to form microfluidic channels.[4] As is known, Raman spectroscopy, as a type of vibrational spectroscopy, is used to measure the difference in energy between incident and inelastically scattered photons due to molecular vibrations[5,6] and is very effective for visualizing and analyzing intrinsic biochemical profiles.[7] Coupled with data analysis tools, this technique has become an effective method for cell phenotyping. For instance, studies on single-cell Raman spectroscopy have shown that cell lines can be distinguished for the analysis of cancer cells[8] with high confidence and high distinguishability in different stages of the disease. Furthermore, many cells can be analyzed by statistical methods such as principal component analysis, support vector machines, decision trees and linear discriminant analysis.

The combination of microfluidic systems with Raman spectroscopy is widely used for molecular detection and *in situ* analysis of biological samples.[9,10] Microfluidic devices help achieve accuracy and reproducibility of results. The microfluidic-based SERS platform starts with the construction of microfluidic devices through microfabrication, and over time, several strategies have been employed to efficiently generate SERS effects in microfluidic systems. Typical applications include analyte detection, SERS-based cell analysis, cell cytometry, liquid chromatography and the construction of integrated microassay platforms.[11–13] It has also been demonstrated that the free-form segmented reflector system for SERS suppresses unwanted background noise, which inherently conforms to the ray-tracing simulation results.[14] In the field of Raman-activated cell sorting, various systems have been demonstrated[15,16] to efficiently implement 'trap-free' continuous flows for cell sorting using Raman signals. In some cases, ultrafast microscopy has also been used instead of the spectroscopic method for cell phenotyping.[17] Furthermore, soft tubular microfluidics and label-free SERS have the potential to detect cells of interest in a dynamic fluid environment.[18]

In this study, a microfluidic chip was developed that allows recording changes in the morphology and state of hemoglobin during erythrocyte trapping. The chip is designed to be capable of: (1) trapping cells, (2) optically monitoring changes in RBC morphology and (3) tracking changes in molecular composition.

A fabricated PDMS chip is shown in Figure 1 along with its 3D model, where the red arrows indicate the direction of flow of RBC suspension. The PDMS microfluidic chip was fabricated using a typical soft lithography technique and glued to a glass substrate. Photolithography and molding were carried out with a negative photoresist SU-8 2025 (25 μm height). We used Sylgard 186 Silicone Elastomer Kit to fabricate a PDMS slab using a standard manufacturing and packaging process for PDMS microfluidics, as shown in Figure 2. Figure 3 shows the COMSOL simulation of the velocity gradient distribution and two RBCs trapped in the mid-section cavity of the chamber.

To validate the microfluidics platform, several generations of design and fabrication were carried out and tested using a

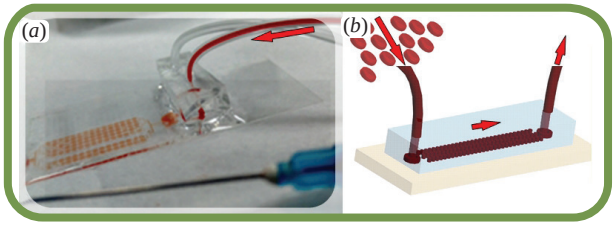

Figure 1 (*a*) Ready-to-use PDMS chip with RBC suspension and 0.6 mm syringe needle shown for scale. (*b*) 3D model of the chip consisting of a PDMS slab (light blue) mounted on a glass slide (light brown) with microfluidic channels filled with RBC suspension (red). Red arrows indicate the direction of flow.

suspension of human RBCs. Through the use of a combination of PDMS and glass, the chip is transparent for optical monitoring. Raman spectroscopy makes it possible to study changes in the internal composition of single RBCs at the molecular level by detecting the porphyrin ring of hemoglobin heme in the spectra. As a proof of concept, we have shown that the prototype device can study the live responses of individual cells to various bio/chemo/physical stimuli.

Raman microspectroscopy was used to study the conformation of RBC hemoglobin heme in a glass–PDMS microfluidic chip.[†] Interaction with chemical bonds causes an energy shift in the scattered light. The resulting Raman spectrum consists of a set of bands, since each band corresponds to a specific chemical bond or group of bonds. The Raman spectrum of erythrocytes basically coincides with the spectrum of hemoglobin heme due to the large amount of hemoglobin in this cell and the high intensity of the heme Raman spectrum. Figure 4[†] shows three examples of Raman spectra of single intact erythrocytes after baseline subtraction. Raman bands correspond to heme (Table 1), and the presence of bands corresponding to both oxygenated and deoxygenated forms of heme means that the hemoglobin of these cells is in a partially oxygenated state.

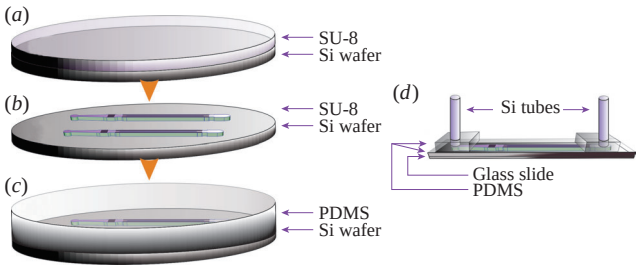

Figure 2 Device fabrication steps: (*a*) application of photoresist SU-8 by spin-coating; (*b*) photolithography and development of SU-8 as the mold insert; (*c*) the PDMS molding process; (*d*) pulling the PDMS out of the silicon wafer, bonding it to a glass slide and attaching the inlet and outlet tubes to complete the chip packaging process.

[†] The Raman spectra of RBCs in a Glass (1.01, 0.17 mm) + PDMS (4.87, 0.13 mm) microfluidic chip were obtained using the complex nanolaboratory NTEGRA Spectra (NT-MDT, Russia) and Nova software (NT-MDT, Russia). An inverted optical microscope Olympus IX71 was used for laser focusing. The NTEGRA spectrometer operated in the confocal mode when recording the spectra. Raman scattering was detected by a CCD camera cooled by a thermoelectric cooling system (Peltier element) down to −50 °C. The incident laser light passed through the glass substrate (1.01 mm), then through an RBC (3–5 μm) and through the PDMS chip (4.87 mm). RBC spectra were collected using a laser with a wavelength of 532 nm and a power of 5.5 mW, a grating of 600 lines mm^{-1} with a spectral resolution of 3.18 cm^{-1}, a ×20 objective with a numerical aperture of 0.45 and a ×100 objective with a numerical aperture of 0.17. One spectrum was recorded for 60 s and the baseline was subtracted using the original Pyraman software and two peaks at 1530 and 1610 cm^{-1} for the porphyrin.

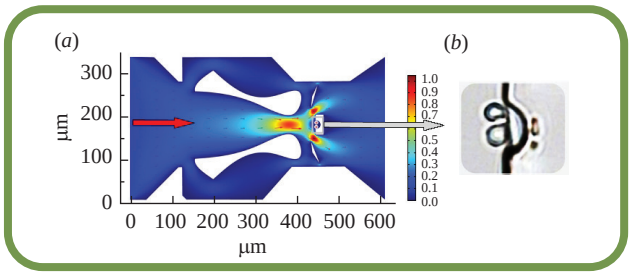

Figure 3 (*a*) COMSOL simulation of a velocity gradient in the trapping chamber (inflow velocity 0.1 m s^{-1}, no-slip boundary condition), with a red arrow indicating flow direction; (*b*) two RBCs trapped in the mid-section cavity of the chamber and ready for tests.

Characteristic bands of stretching vibrations of the heme of hemoglobin were found in the region of 1000–1700 cm^{-1} of the Raman spectrum of erythrocytes (see Figure 4). The bands at 1550, 1585 and 1637 cm^{-1} refer to vibrations of methine bridges, the peaks at 1335 and 1375 cm^{-1} illustrate symmetrical vibrations of the pyrrole rings, and the peak at 1172 cm^{-1} is due to asymmetric vibrations of the pyrrole rings. We have found that with an increase in pO_2 in media in the range from 5.0 to 159.6 mm Hg, the amplitude of the bands at 1355, 1375, 1552 and 1637 cm^{-1} of the Raman spectrum changes. These changes correspond to the deformation of the heme porphyrin ring due to the binding of oxygen to the iron ion in the heme center. The position of the peaks at 1355–1375 cm^{-1} is sensitive to the presence of the ligand. The binding of oxygen pulls the electron density off the pyrrole rings and causes the peak to shift to 1375 cm^{-1}. The high-frequency group of peaks is sensitive to the spin state of iron (the size of the iron ion) and the diameter of the porphyrin ring. If the diameter of the iron increases due to the high spin state of iron in deoxygenated hemoglobin, then the ring is deformed, the bond lengths increase, and the position of the band shifts to a lower frequency.

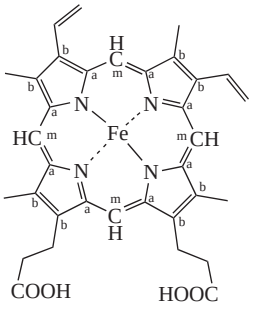

This result indicates that the Raman spectroscopy data obtained during the movement and arrest of erythrocytes can be used to assess not only the change in the hemoglobin heme conformation upon O_2 binding, but also the redistribution of cells with oxidized

Table 1 Assignment of Raman bands in the hemoglobin spectrum.[19–22]

Raman shift /cm^{-1}	Chemical bonds	Band sensitivity
1640	C^aC^m, C^aC^mH, C^aC^b	Redox and spin state of Fe, ligand binding
1580–1588	C^aC^m, C^aC^mH	Spin state of heme Fe, porphirin ring diameter
1552	C^aC^m, C^aC^mH	Spin state of heme Fe, porphirin ring diameter
1375	C^aC^b, C^aN, NC^aN	Redox state of Fe, ligand binding (for HbO_2)
1355	C^aC^b, C^aN, NC^aN	Redox state of Fe, ligand binding (for dHb)

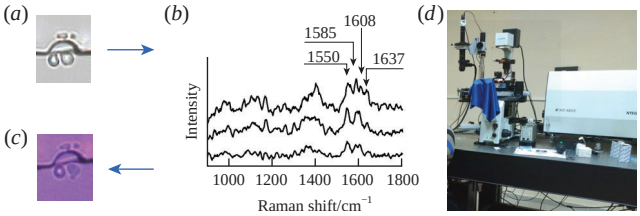

Figure 4 Photomicrographs of trapped erythrocytes (*a*) before and (*c*) after exposure to laser light; (*b*) three examples of Raman spectra of single intact erythrocytes after baseline subtraction; (*d*) photograph of the test bench of the NTEGRA Spectra nanolaboratory controlled by Nova software.

and reduced hemoglobin, as well as to control the redistribution of oxygen concentration from cell to cell. The platform allows recording the state of hemoglobin in erythrocytes and can be improved by additional coating of the trapping layer with silver nanoparticles. This will significantly increase the resolution of the method and reduce the signal recording time, which is important for the functional state of the cell.[23,24]

Our microfluidic device, coupled with a Raman spectrometer, has the potential to sort and study young and old erythrocytes (different traps can capture cells of different sizes), as well as observe the response of single RBCs to new drugs by washing them with a test solution and monitoring the cell responses using optical microscopy and Raman spectroscopy.[25] Furthermore, the design of this microfluidic platform allows research on the hydrodynamic behavior of old/abnormal/damaged/infected cells.

G.V.M. and E.U.P. acknowledge the partial support from the Russian Science Foundation (grant no. 19-79-30062).

References

1 M. A. Haque, H. D. Espinosa and H. J. Lee, *MRS Bull.*, 2010, **35**, 375.
2 R. Nosrati, P. J. Graham, B. Zhang, J. Riordon, A. Lagunov, T. G. Hannam, C. Escobedo, K. Jarvi and D. Sinton, *Nat. Rev. Urol.*, 2017, **14**, 707.
3 Y. Alapan, J. A. Little and U. A. Gurkan, *Sci. Rep.*, 2014, **4**, 7173.
4 P. Xue, Q. Li, Y. Li, L. Sun, L. Zhang, Z. Xu and Y. Kang, *ACS Appl. Mater. Interfaces*, 2017, **9**, 33632.
5 D. Wang, P. He, Z. Wang, G. Li, N. Majed and A. Z. Gu, *Curr. Opin. Biotechnol.*, 2020, **64**, 218.
6 Y. He, X. Wang, B. Ma and J. Xu, *Biotechnol. Adv.*, 2019, **37**, 107388.
7 Y. Song, H. Yin and W. E. Huang, *Curr. Opin. Chem. Biol.*, 2016, **33**, 1.
8 J. Gala de Pablo, F. J. Armistead, S. A. Peyman, D. Bonthron, M. Lones, S. Smith and S. D. Evans, *J. Raman Spectrosc.*, 2018, **49**, 1323.
9 G. Ochoa-Vazquez, B. Kharisov, A. Arizmendi-Morquecho, A. Cario, C. Aymonier, S. Marre and I. López, *IEEE Transactions on NanoBioscience*, 2019, **18**, 558.
10 D. Uzunoglu, M. Altunbek, G. Kuku and M. Culha, in *Single-Cell Omic: Technological Advances and Applications*, eds. D. Barh and V. Azevedo, Academic Press, London, 2019, vol. 1, pp. 153–177.
11 A. Tycova, J. Prikryl and F. Foret, *Electrophoresis*, 2017, **38**, 1977.
12 K. S. Lee, M. Palatinszky, F. C. Pereira, J. Nguyen, V. I. Fernandez, A. J. Mueller, F. Menolascina, H. Daims, D. Berry, M. Wagner and R. Stocker, *Nat. Microbiol.*, 2019, **4**, 1035.
13 C. Dallari, C. Credi, E. Lenci, A. Trabocchi, R. Cicchi and F. S. Pavone, *JPhys Photonics*, 2020, **2**, 024008.
14 Q. Liu, M. Stenbæk Schmidt, H. Thienpont and H. Ottevaere, *Sensors*, 2020, **20**, 1250.
15 D. McIlvenna, W. E. Huang, P. Davison, A. Glidle, J. Cooper and H. Yin, *Lab Chip*, 2016, **16**, 1420.
16 V. O. Baron, M. Chen, B. Hammarstrom, R. J. H. Hammond, P. Glynne-Jones, S. H. Gillespie and K. Dholakia, *Commun. Biol.*, 2020, **3**, 236.
17 N. Nitta, T. Iino, A. Isozaki, M. Yamagishi, Y. Kitahama, S. Sakuma, Y. Suzuki, H. Tezuka, M. Oikawa, F. Arai, T. Asai, D. Deng, H. Fukuzawa, M. Hase, T. Hasunuma, T. Hayakawa, K. Hiraki, K. Hiramatsu, Y. Hoshino, M. Inaba, Y. Inoue, T. Ito, M. Kajikawa, H. Karakawa, Y. Kasai, Y. Kato, H. Kobayashi, C. Lei, S. Matsusaka, H. Mikami, A. Nakagawa, K. Numata, T. Ota, T. Sekiya, K. Shiba, Y. Shirasaki, N. Suzuki, S. Tanaka, S. Ueno, H. Watarai, T. Yamano, M. Yazawa, Y. Yonamine, D. Di Carlo, Y. Hosokawa, S. Uemura, T. Sugimura, Y. Ozeki and K. Goda, *Nat. Commun.*, 2020, **11**, 3452.
18 X. Xu, L. Zhao, Q. Xue, J. Fan, Q. Hu, C. Tang, H. Shi, B. Hu and J. Tian, *Anal. Chem.*, 2019, **91**, 7973.
19 P. Stein, J. M. Burke and T. G. Spiro, *J. Am. Chem. Soc.*, 1975, **97**, 2304.
20 T. Kitagawa, Y. Kyogoku, T. Iizuka and M. I. Saito, *J. Am. Chem. Soc.*, 1976, **98**, 5169.
21 S. Choi, T. G. Spiro, K. C. Langry, K. M. Smith, D. L. Budd and G. N. La Mar, *J. Am. Chem. Soc.*, 1982, **104**, 4345.
22 B. R. Wood, P. Caspers, G. J. Puppels, S. Pandiancherri and D. McNaughton, *Anal. Bioanal. Chem.*, 2007, **387**, 1691.
23 E. I. Nikelshparg, V. G. Grivennikova, A. A. Baizhumanov, A. A. Semenova, V. Sosnovtseva, E. A. Goodilin, G. V. Maksimov and N. A. Brazhe, *Mendeleev Commun.*, 2019, **29**, 635.
24 N. A. Brazhe, K. Thomsen, M. Lønstrup, A. R. Brazhe, E. I. Nikelshparg, G. V. Maksimov, M. Lauritzen and O. Sosnovtseva, *J. Biophotonics*, 2018, **11**, e201700311.
25 A. V. Vlasov, N. L. Maliar, S. V. Bazhenov, E. I. Nikelshparg, N. A. Brazhe, A. D. Vlasova, S. D. Osipov, V. V. Sudarev, Y. L. Ryzhykau, A. O. Bogorodskiy, E. V. Zinovev, A. V. Rogachev, I. V. Manukhov, V. I. Borshchevskiy, A. I. Kuklin, J. Pokorný, O. Sosnovtseva, G. V. Maksimov and V. I. Gordeliy, *Crystals*, 2020, **10**, 38.

Received: 17th December 2021; Com. 21/6777